2021 43rd Annual International Conference of the
IEEE Engineering in Medicine & Biology Society (EMBC)
Oct 31 - Nov 4, 2021. Virtual Conference

The Imaging of Magnetic Nanoparticles with Low-power Magneto-acoustic Tomography

Zijian Gao, Peng Ge, Yifei Xu, Xiaopeng Yu, Feng Gao and Fei Gao*, *Member, IEEE*

***Abstract*— The magnetic nanoparticles have been widely explored as an important kind of biomaterial for the treatment and diagnosis of cancer. Imaging of magnetic nanoparticles can greatly facilitate treatment and diagnosis in both preclinical and clinical applications. The magnetoacoustic tomography is a non-invasive imaging modality for the distribution of the magnetic nanoparticles. However, the traditional magnetoacoustic imaging system requires higher power and the large instantaneous current that suffers cost and safety issues. In this paper, we propose a low-power magnetoacoustic tomography system, whose power amplifier only has 30 W peak power. The system used a pulse train of excitation to gain energy accumulation by resonance. The reconstructed algorithm, i.e. universal back-projection, was applied for imaging. To prove the feasibility and potential of the proposed system, we performed the imaging experiments with the gelatin phantom containing the magnetic nanoparticles.**

I. Introduction

Nowadays, the nanoscience has been one of the most important research area [1]. Among them, the magnetic nanoparticles (MNPs) exhibit small size and excellent physicochemical properties. Thus, MNPs show the enormous potential for vast fields of biotechnology, material science, and environmental engineering areas. In biomedical applications, the magnetic nanoparticles can be applied to the treatment and diagnosis of cancer. For example, therapeutic drugs can be loaded on the MNPs and released by the excitation with magnetic control until the nanoparticles arrive at the tumors site with blood circulation [2]. Therefore, the imaging of the distribution of the MNPs is significant for many clinical treatment and diagnosis.

The main ingredient of the magnetic nanoparticle is iron oxide (Fe_3O_4 and Fe_2O_3). It's possible to use magnetic resonance imaging (MRI) for imaging of the MNPs. MRI can provide high resolution distribution, but the limitations are sensitivity and the cost of large-scale applications [3, 4]. In recent years, magnetoacoustic tomography (MAT) has been applied for imaging of MNPs [5-7]. The MAT is a non-invasive imaging modality, which combines the specific absorption contrast of MNPs with the advantages of high-resolution ultrasound detection in deep tissue [8-12]. The MAT applies the pulsed alternating magnetic field to induce magneto-motive force in the object, e.g. MNPs. The acoustic vibrations could be excited by the force with the same frequency as the pulsed alternating magnetic field. This frequency matches the range of ultrasound frequency. Thus, the acoustic vibrations can generate ultrasound signals, which can be detected by the ultrasound transducer. Then, the reconstructed algorithm can be used to obtain the distribution of MNPs.

However, the conventional MAT system needs the high-power short-pulse radio frequency (RF) current in coils to excite the pulsed alternating magnetic field. Generally speaking, the strong magnetoacoustic signals require the high-voltage (~24 kV) microsecond pulse and pulse current (~600 A) [13-15]. Such high energy RF excitation sources are usually expensive with safety problem.

In this paper, we developed a lower power MAT system with a lower power amplifier (30 W) for imaging of the distribution of MNPs. The excitation source is a low power sinusoidal pulse train. By raster scanning of ultrasound transducer and image reconstruction, imaging of the MNPs is well demonstrated.

II. Theory

The schematic diagram of the MAT is shown in Fig. 1. MNPs form a fluid and are embedded in biological tissue. Meanwhile, MNPs lie in the pulsed alternating magnetic B. Since the interaction of the pulsed alternating magnetic and magnetic dipoles of the MNPs, the pulsed magneto-motive force generated in this process can cause MNPs' acoustic vibrations. This acoustic vibration propagates in all directions of the tissue medium with the same frequency as the pulsed alternating magnetic.

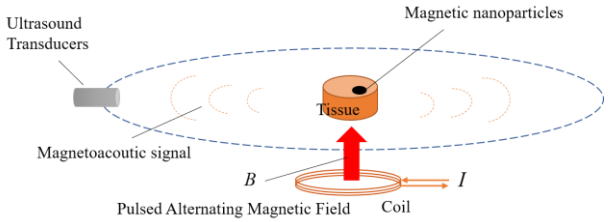

Figure 1. The schematic diagram of the magnetoacoustic tomography.

The pulsed alternating magnetic field B can be stimulated by the short-pulse radio frequency current in the coil, which is a time-varying magnetic field. The magneto-motive force is:

$$F = \frac{\chi_m V_m f_m}{2\mu} \nabla(B^2) \tag{1}$$

Where χ_m is magnetic susceptibility of MNPs, V_m and f_m indicate the volume and the volume fraction of the MNPs,

Zijian Gao, Peng Ge, Yifei Xu, Xiaopeng Yu, Feng Gao and Fei Gao are with the Hybrid Imaging System Laboratory, Shanghai Engineering Research Center of Intelligent Vision and Imaging, Shanghai Engineering Research Center of Energy Efficient and Custom AI IC, School of Information Science and Technology, ShanghaiTech University, Shanghai 201210, China (*corresponding author: gaofei@shanghaitech.edu.cn).

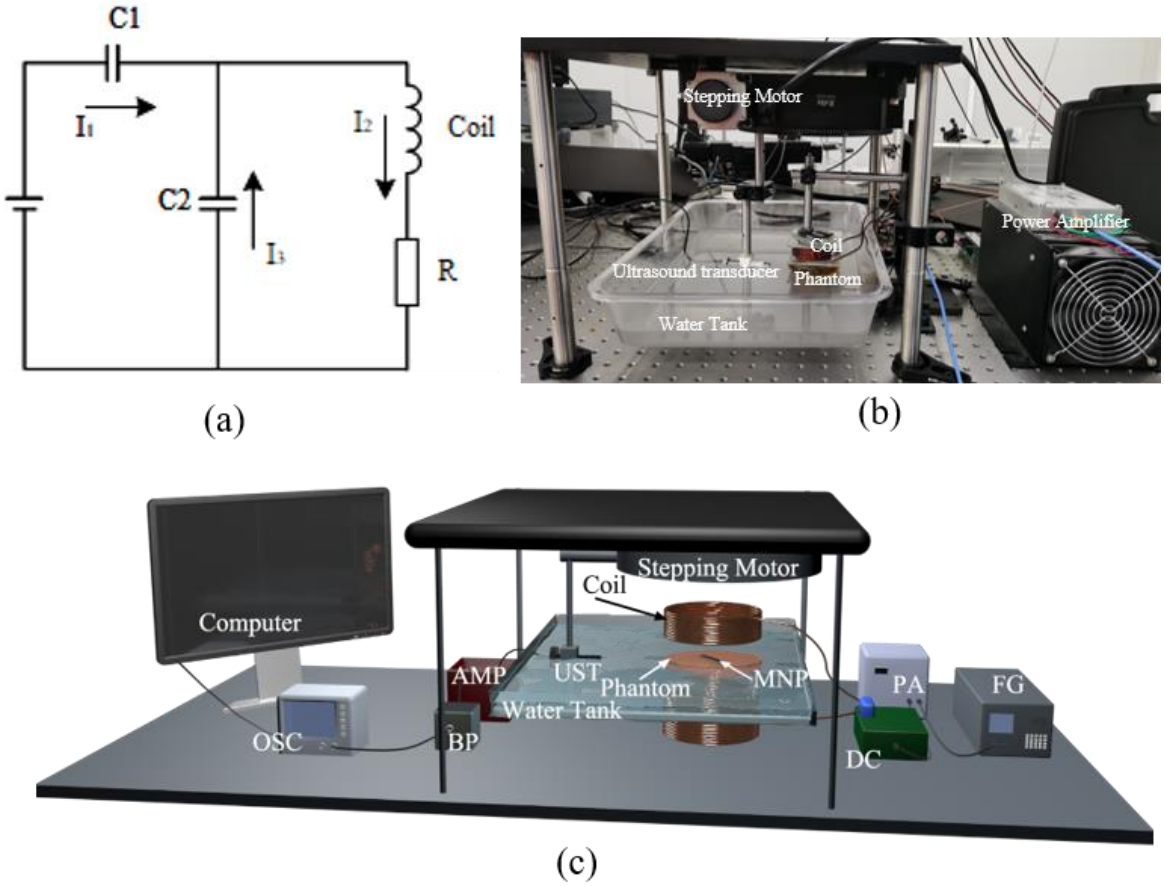

Figure 2. (a) The dual capacitor resonance circuit C1=C2=1 nF, R=0.1 Ω, the resonance frequency is 1.1 MHz. (b) Photography of the MAT system. (c) Detailed experiment setup of MAT system, PA: power amplifier; FG: function generator; DC: driving circuit; UST: ultrasound transducer; AMP: amplifier; BP: bandpass filter; OSC: oscilloscope.

μ is the magnetic permeability. The MNPs will vibrate under magneto-motive force, and ultrasound wave can be generated by the above-mentioned acoustic vibration, which is so-called MA signal. The wave equation of the MA signal is derived as:

$$\nabla^2 p - \frac{1}{c^2}\frac{\partial^2 p}{\partial t^2} = \nabla \cdot F \tag{2}$$

where p is acoustic pressure and c is the sound speed of 1500m/s for the tissue. We suppose the magnetic field on the MNPs is consistent. Then the solution of the wave equation by the Green function method with the zero-initial-value condition and the ultrasound pressure at position r can be formed as:

$$p(r,t) = -\frac{1}{4\pi}\iiint \frac{\nabla \times F(r,t')}{|r-r'|} dV \Bigg|_{t'=t-\frac{|r-r'|}{c}} \tag{3}$$

Furthermore, the MA signals can be detected by ultrasound detectors, followed by image reconstruction. In this paper, the universal back-projection algorithm is applied to reconstruct the distribution of the acoustic source, which reflects the distribution of the MNPs [16].

III. METHODS

A. Experiment setup

Since the intensity of the MA signal depends on the intensity of the pulsed alternating magnetic field, the dual capacitor resonance circuit, as show in Fig. 2(a), can be used as a driving circuit to enhance the MA signal's intensity [17]. The resonance frequency of the driving circuit is 1.1 MHz. With the low-power (30 W) amplifier, the resonance current can achieve the level of > 10 A.

Fig. 2(b)-(c) show the diagram of the experimental setup. On the upper and lower sides of the water tank, a couple of coils constitute the Helmholtz coil. Each coil is 6 cm diameter and 10 turns, which is made in a 3 mm diameter copper wire by hand. The coils are connected to the driving circuit. From the driving circuit, the resonance current will feed into the coils to generate pulsed alternating magnetic fields. The power amplifier (30 W, LZY- 22+, Mini-Circuits.) outputs excitation current to the driving circuit, and the input signals of the amplifier are from the function generator (DG5352, RIGOL). The input signals are a series of sinusoidal pulses with 15 cycles and 10 ms repeat period. These signals have the same frequency as the resonance frequency (1.1 MHz) of the coil. It will stimulate the resonance circuit to accumulate energy, and generate higher current and stronger magnetic field.

Both the phantom of the tissue with the MNPs and the single-point ultrasound transducer (HFC076, Doppler Inc.) are immersed in the water. The center frequency of the ultrasound transducer is 2.25 MHz. The transducer is connected with a rotating platform. Driven by a stepping motor (RAP200, Zolix Inc.), the MA signals can be detected over the 180 degrees with a step size of 6 degrees around the MNPs by the transducer. Then, the MA signals will be amplified with a signal amplifier (AMP-16, Photosound Inc.), and filtered with a bandpass filter with the 1 MHz center frequency and 110 kHz bandwidth.

B. Signal processing

A typical measured MA signal is showed in Fig. 3. This MA signal is collected by the ultrasound transducer with the processing of amplifying and filtering, followed by 100 times average to suppress random noise. It shows that the MA signal has quite good signal-to-noise ratio (SNR).

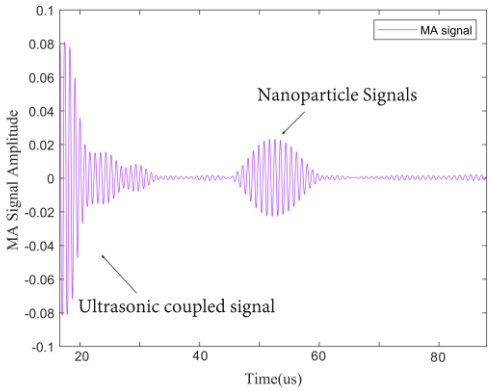

Figure 3. The magnetoacoustic signals of the magnetic nanoparticles.

However, the generation of MA signal needs the energy accumulation by a series of cyclic pulses, since the lower power of the individual pulse. Thus, the received MA signal has poor axial resolution compared with conventional single-pulse MA signal. The advantage is that the intensity of MA signal is gradually increasing with higher SNR. Using this feature, we can simply process the MA signal to improve the axial resolution, as show in Fig. 4. In Fig. 4(b), the Hilbert transformation can be applied to obtain the envelope of MA signals. From the envelope curve, the position of extreme point of the MA signals intensity can be obtained. We can intercept the signal of one period near this location, which are the main MA signals and contains amplitude and phase information. The envelope of the main MA signals can replace the original MA signals with this processed signals, which can improve the axial resolution, as showed in Fig. 4(c)-(d).

After the process of the detection over the 180 degrees with a step size of 6 degrees, the data can be saved in the computer from the oscilloscope. Then reconstructed algorithm of the universal back-projection will be applied to get the imaging of the distribution of MNPs.

IV. Results

We executed the magnetoacoustic tomography experiments with homemade gelatin phantom using the proposed low-power MAT system. We build a cylindrical gelatin phantom for simulating biological tissue. The phantom is 65 mm in diameter and 20 mm in height, and has a gelatin concentration of 10%. In the center of the gelatin phantom, there is a hole with ~50 mm wide and 10 mm deep, which is made to load the target. The target is ferrofluid whose concentration is ~ 300 mg/ml with MNPs. The main components of the MNPs is Fe_3O_4 and Fe_2O_3. The ferrofluid filled the hole in the middle of the gelatin phantom, which is showed in Fig. 5(a).

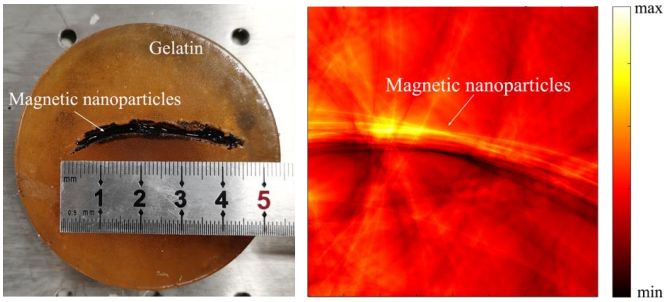

Figure 5. (a) Photograph of the gelatin phantom with magnetic nanoparticle target. (b) Reconstructed image of the target shown in (a).

In the experiment, the phantom was immersed in a water tank and lied in the center of the Helmholtz coil. A series of sinusoidal pulses (15 cycles, 1.1 MHz) were generated by function generator and fed into the power amplifier (30 W). The output signals of the power amplifier drove the resonant circuit to stimulate the pulsed alternating magnetic field in the Helmholtz coil. Then the pulsed alternating magnetic field interact with the magnetic dipoles of the MNPs so that magnetomotive force acting on MNPs. After this process, the MNPs generated acoustic vibration with the 1.1 MHz resonant frequency and produced the ultrasound signals of the same frequency, which were MA signals. The MA signals were collected by the single ultrasound transducer with 180 degrees over the target. Then the reconstructed algorithm, universal back-projection, was used in the imaging experiment in MATLAB. The imaging result is shown in Fig. 5(b).

From the imaging result, we can find the approximate distribution profile and position of magnetic nanoparticles, which are elongated in the center of the field of view. Therefore, the experimental result verified the feasibility and potential of the proposed low-power MAT system.

V. Conclusions

In this paper, a lower-power MAT system is proposed. We introduced the experiment setup of the MAT system with the lower power amplifier (30 W). Then we performed the phantom experiment with the magnetic nanoparticles in gelatin phantom. The system exhibits low cost and low power, which is safe and economical compared with conventional high-power MAT. The imaging result also shows good spatial resolution. This method proved feasibility and potential of imaging distribution of magnetic nanoparticles in biological tissue

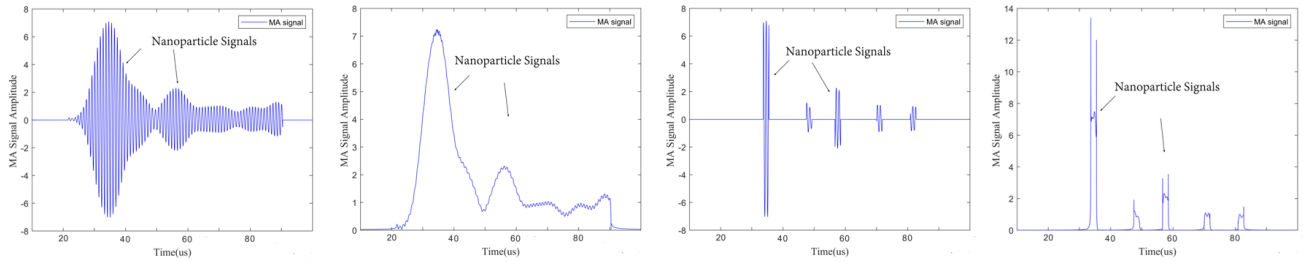

Figure 4. (a) The original MA signals. (b) The envelope of the MA signals. (c) The main MA signals. (d) The envelope of the main MA signals.

with a low power and portable system. In the future work, the real-time MAT system will be performed for in vivo imaging scenarios.

ACKNOWLEDGMENT

This research was funded by National Natural Science Foundation of China (61805139).

REFERENCES

[1] A. Akbarzadeh, M. Samiei, and S. Davaran, "Magnetic nanoparticles: preparation, physical properties, and applications in biomedicine," *Nanoscale Res Lett,* vol. 7, no. 1, pp. 144, Feb 21, 2012.

[2] S. Gul, S. B. Khan, I. U. Rehman, M. A. Khan, and M. Khan, "A comprehensive review of magnetic nanomaterials modern day theranostics," *Frontiers in Materials,* vol. 6, pp. 179, 2019.

[3] M. L. Etheridge, K. R. Hurley, J. Zhang, S. Jeon, H. L. Ring, C. Hogan, C. L. Haynes, M. Garwood, and J. C. Bischof, "Accounting for biological aggregation in heating and imaging of magnetic nanoparticles," *Technology (Singap World Sci),* vol. 2, no. 3, pp. 214-228, Sep, 2014.

[4] J. J. Zhang, R. Chamberlain, M. Etheridge, D. Idiyatullin, C. Corum, J. Bischof, and M. Garwood, "Quantifying Iron-Oxide Nanoparticles at High Concentration Based on Longitudinal Relaxation Using a Three-Dimensional SWIFT Look-Locker Sequence," *Magnetic Resonance in Medicine,* vol. 71, no. 6, pp. 1982-1988, Jun, 2014.

[5] G. Hu, and B. He, "Magnetoacoustic imaging of magnetic iron oxide nanoparticles embedded in biological tissues with microsecond magnetic stimulation," *Applied Physics Letters,* vol. 100, no. 1, Jan 2, 2012.

[6] X. Li, K. Yu, and B. He, "Magnetoacoustic tomography with magnetic induction (MAT-MI) for imaging electrical conductivity of biological tissue: a tutorial review," *Phys Med Biol,* vol. 61, no. 18, pp. R249-R270, Sep 21, 2016.

[7] S. Y. Liu, R. C. Zhang, Y. Q. Luo, and Y. J. Zheng, "Magnetoacoustic microscopic imaging of conductive objects and nanoparticles distribution," *Journal of Applied Physics,* vol. 122, no. 12, Sep 28, 2017.

[8] X. Li, and B. He, "Magnetoacoustic Tomography with Magnetic Induction (MAT-MI) for Electrical Conductivity Imaging," *2009 Annual International Conference of the Ieee Engineering in Medicine and Biology Society, Vols 1-20*, pp. 3173-3176, 2009.

[9] L. Mariappan, X. Li, and B. He, "B-Scan Based Acoustic Source Reconstruction for Magnetoacoustic Tomography With Magnetic Induction (MAT-MI)," *Ieee Transactions on Biomedical Engineering,* vol. 58, no. 3, pp. 713-720, Mar, 2011.

[10] X. D. Sun, Y. Q. Zhou, Q. Y. Ma, and D. Zhang, "Radiation theory comparison for magnetoacoustic tomography with magnetic induction (MAT-MI)," *Chinese Science Bulletin,* vol. 59, no. 26, pp. 3246-3254, Sep, 2014.

[11] X. H. Yan, Y. Pan, W. H. Chen, Z. Y. Xu, and Z. X. Li, "Simulation research on the forward problem of magnetoacoustic concentration tomography for magnetic nanoparticles with magnetic induction in a saturation magnetization state," *Journal of Physics D-Applied Physics,* vol. 54, no. 7, Feb 18, 2021.

[12] L. A. Zhou, X. Li, S. N. Zhu, and B. He, "Magnetoacoustic tomography with magnetic induction (MAT-MI) for breast tumor imaging: numerical modeling and simulation," *Physics in Medicine and Biology,* vol. 56, no. 7, pp. 1967-1983, Apr 7, 2011.

[13] Y. Kai, S. Qi, S. Ashkenazi, J. C. Bischof, and H. Bin, "In Vivo Electrical Conductivity Contrast Imaging in a Mouse Model of Cancer Using High-Frequency Magnetoacoustic Tomography With Magnetic Induction (hfMAT-MI)," *IEEE Trans Med Imaging,* vol. 35, no. 10, pp. 2301-2311, Oct, 2016.

[14] L. Mariappan, Q. Shao, C. L. Jiang, K. Yu, S. Ashkenazi, J. C. Bischof, and B. He, "Magneto acoustic tomography with short pulsed magnetic field for in-vivo imaging of magnetic iron oxide nanoparticles," *Nanomedicine-Nanotechnology Biology and Medicine,* vol. 12, no. 3, pp. 689-699, Apr, 2016.

[15] A. R. Zywica, M. Ziolkowski, and S. Gratkowski, "Detailed Analytical Approach to Solve the Magnetoacoustic Tomography with Magnetic Induction (MAT-MI) Problem for Three-Layer Objects," *Energies,* vol. 13, no. 24, Dec, 2020.

[16] M. H. Xu, and L. H. V. Wang, "Universal back-projection algorithm for photoacoustic computed tomography," *Physical Review E,* vol. 71, no. 1, Jan, 2005.

[17] Y. F. Xu, H. T. Zhong, D. H. Jiang, and F. Gao, "Low-power magnetoacoustic sensing with 30W power amplifier," *Proceedings of the 2019 Ieee Asia-Pacific Microwave Conference (Apmc)*, pp. 1164-1166, 2019.